

Calculation of radiative corrections to hyperfine splittings in the neutral alkali metals

J. Sapirstein*

Department of Physics, University of Notre Dame, Notre Dame, Indiana 46556

K. T. Cheng†

University of California, Lawrence Livermore National Laboratory, Livermore, California 94550

(Received 4 November 2002; published 28 February 2003)

The radiative correction to hyperfine splitting in hydrogen is dominated by the Schwinger term, $\alpha/2\pi E_F$, where E_F is the lowest-order hyperfine splitting. Binding corrections to this term, which enter as powers and logarithms of $Z\alpha$, can be expected to be increasingly important in atoms with higher nuclear charge Z . Methods that include all orders of $Z\alpha$, developed first to study highly charged ions, are adapted to the study of the neutral alkali metals, lithium through francium. It is shown that the use of the Schwinger term alone to account for radiative corrections to hyperfine splittings becomes qualitatively incorrect for the heavier alkali metals.

DOI: 10.1103/PhysRevA.67.022512

PACS number(s): 31.30.Jv, 32.10.Fn, 12.20.Ds

I. INTRODUCTION

The study of radiative corrections in atoms and ions has a lengthy history. It was realized early on by Wichmann and Kroll [1] for vacuum polarization and by Brown and Mayers [2] for the self-energy that the power series expansion in $Z\alpha$ used in the study of the Lamb shift in hydrogen would converge slowly at high Z , and they studied the Lamb shift to all orders of $Z\alpha$ using exact Dirac-Coulomb propagators. This approach has been developed to an extremely precise level over the years by Mohr and collaborators, culminating in a recent work in which the one-loop self-energy of neutral hydrogen has been evaluated to an accuracy of 1 Hz [3].

More recently the numerical techniques first applied to the Lamb shift have been extended to the study of radiative corrections to hyperfine splittings (hfs) [4], which enter as powers of α multiplying the lowest-order hfs energy E_F . Measurements of the ground-state hfs in hydrogenlike ions such as $^{209}\text{Bi}^{82+}$ [5] also make all-order studies of binding corrections to the leading Schwinger term [6], $\alpha/2\pi E_F$, of interest. As could be expected from the formula that includes first-order binding corrections [7],

$$\nu = E_F \left[\frac{\alpha}{2\pi} + Z\alpha^2 \left(\ln 2 - \frac{5}{2} \right) \right], \quad (1)$$

which changes sign near $Z=12$, the use of the Schwinger term alone, which gives a constant value of $+0.5$ in units of $\alpha/\pi E_F$, to describe radiative corrections to hfs is qualitatively incorrect for mid- to high- Z ions. Indeed, for hydrogenlike bismuth, the inclusion of the leading binding correction in Eq. (1) gives -2.94 in the same units, while the exact calculations further change the result to -2.23 [4]. We note that were the next term in the $Z\alpha$ expansion [8] to be used for hydrogenlike bismuth, a completely incorrect value of

$+2.62$ would result, so the rough agreement of the exact calculation with the first two terms of the $Z\alpha$ expansion is accidental.

The confirmation of this striking effect has unfortunately been obscured by nuclear physics uncertainties: the large overlap of the electron with the nucleus of a high- Z ion leads to a Bohr-Weisskopf (BW) contribution [9], which comes from the finite distribution of the nuclear magnetization current, about twice as large as the quantum electrodynamic (QED) correction. In fact, one nuclear calculation of this effect for the ground-state hfs of $^{209}\text{Bi}^{82+}$ leads to agreement with experiment only if the QED correction is neglected [10]. It is possible to greatly reduce the nuclear physics uncertainty by also measuring the ground-state hfs in lithiumlike bismuth, a point made in Ref. [11]. In that paper, the measurement of the $1s$ hfs of hydrogenlike bismuth was used to make an unambiguous prediction of the $2s$ hfs of lithiumlike bismuth: these results were confirmed in Ref. [12]. The ground-state hfs for lithiumlike bismuth has been measured in an EBIT experiment [13], but with a precision too low to detect the radiative corrections.

In this paper, we apply the techniques developed to calculate radiative corrections to hfs in lithiumlike bismuth to the ground-state hfs of neutral alkali metals. This parallels the approach of a previous paper [14], where we extended techniques for the evaluation of the Lamb shift in highly charged ions to the same atoms. Whereas in that paper the radiative corrections to the Lamb shift were quite small, our main result here is that for the heavier alkali metals, a significant enhancement of the Schwinger correction is present, sufficiently large so that it cannot be ignored in accurate calculations of hfs.

II. THEORY

Our calculations are carried out in Furry representation QED with a local potential based on density-functional theory, the Kohn-Sham potential, given by

*Email address: jsapirst@nd.edu

†Email address: ktcheng@llnl.gov

TABLE I. One-photon exchange contributions to hfs in the alkali metals. ΔExpt is the difference between theory (Sum) and experiment and Breit-QED is the difference between ν^{1E} and first-order MBPT: Units MHz.

	⁷ Li	²³ Na	³⁹ K	⁸⁷ Rb	¹³³ Cs	²¹² Fr
Nuclear moment	3.25643	2.21752	0.391466	2.75182	2.58203	4.62
Nuclear spin	3/2	3/2	3/2	3/2	7/2	5
Experiment	803.504 ^a	1771.631 ^a	461.720 ^a	6834.683 ^a	9192.632 ^a	36257 ^b
$\nu^{(0)}$	725.056	1499.042	343.478	4886.320	6164.831	31467
ν^{BW}	-0.079	-0.737	-0.352	-15.062	-43.936	-851
ν^{1E}	44.631	134.506	53.305	1064.727	1687.852	14600
Sum	769.608	1632.811	396.431	5935.985	7808.747	45216
ΔExpt	33.896	138.820	65.289	898.698	1383.885	-8959
1st-order MBPT	44.549	134.187	53.255	1065.925	1694.332	14743
Breit-QED	0.082	0.319	0.050	-1.198	-6.480	-143

^aReference [17].

^bReference [18].

$$U(r) = -\frac{Z_{\text{eff}}(r)\alpha}{r}, \quad (2)$$

with

$$Z_{\text{eff}}(r) = Z_{\text{nuc}}(r) - r \int_{r>} dr' \frac{1}{r'} \rho_t(r') + \frac{2}{3} \left[\frac{81r\rho_t(r)}{32\pi^2} \right]^{1/3}, \quad (3)$$

where $\rho_t(r)$ is the total charge density. To maintain the correct asymptotic limit of $Z_{\text{eff}}(r) \rightarrow 1$ for neutral atoms, $Z_{\text{eff}}(r)$ is set to 1 once the above formula reduces to that value at large r . Natural units in which $\hbar = c = 1$ are used here.

The matrix element of the hyperfine interaction is defined as

$$V_{ij} \equiv \int d^3r \bar{\psi}_i(\vec{r}) V(\vec{r}) \psi_j(\vec{r}), \quad (4)$$

with

$$V(\vec{r}) = -e \vec{\gamma} \cdot \vec{A}(\vec{r}) = -e \vec{\gamma} \cdot \frac{\vec{\mu} \times \vec{r}}{4\pi r^3} F_{\text{BW}}(r). \quad (5)$$

The lowest-order hfs of a valence state v can then be obtained from V_{vv} as $E_F = \nu^{(0)} = V_{vv}(2I+1)/I$, where I is the nuclear spin and we have used the fact that we consider only s states here.

The function $F_{\text{BW}}(r)$ models the distribution of nuclear magnetism. It will be taken to be unity for all calculations except the lowest-order one. As noted above, uncertainties in this distribution play an important role in highly charged hydrogenlike and lithiumlike bismuth, and we will discuss its role in the neutral alkali metals in the conclusion. Here we simply take a uniform distribution,

$$F_{\text{BW}}(r) = \begin{cases} (r/R)^3 & r < R \\ 1 & r \geq R, \end{cases} \quad (6)$$

with R chosen to give the same root-mean-square (rms) radius as the charge distribution. We take the nuclear moments from the table of isotopes [15] and the rms radii from the compilation of Johnson and Soff [16]. Nuclear moments, spins, and experimental hfs for the atoms considered here are tabulated in the first three rows of Table I. The experimental values are all taken from Ref. [17] with the exception of francium [18].

We now define the hyperfine splitting as

$$\nu = \nu^{(0)} + \nu^{\text{BW}} + \nu^{1E} + \nu^{2E+} + \nu^{\text{VP}} + \nu^{\text{SE}}. \quad (7)$$

The first term $\nu^{(0)}$ in Eq. (7) is the lowest-order hfs with $F_{\text{BW}}=1$, and the second term ν^{BW} accounts for the change when the uniform magnetization distribution described above is used. They are tabulated in the fourth and fifth rows of Table I, respectively. The following term ν^{1E} includes the effect of one-photon exchange on hfs and is calculated in the following section. Higher-order correlation corrections with two- and more-photon exchanges are given in ν^{2E+} , which plays an important role in comparing theory and experiment that will be discussed in the conclusion. The last two terms, vacuum polarization ν^{VP} and self-energy ν^{SE} contributions to hfs, are the main focus of this paper and will be treated in Sec. IV.

III. ONE-PHOTON EXCHANGE

In this section, we calculate the QED counterpart of first-order many-body perturbation theory (MBPT), and show that the result is close to, but for the heavier alkali metals noticeably different from, MBPT. The use of a non-Coulomb local potential $U(r)$ leads to a counter potential $\tilde{U}(r)$ in perturbation calculations,

$$\tilde{U}(r) = [Z_{\text{nuc}}(r) - Z_{\text{eff}}(r)]\alpha/r. \quad (8)$$

First-order correlation diagrams from the counter potential and one-photon exchange are shown in Fig. 1 and the associated formulas are

$$\begin{aligned}
 \nu^{1E} = & - \sum_i^{i \neq v} \frac{V_{vi} \tilde{U}_{iv}}{\epsilon_v - \epsilon_i} - \sum_i^{i \neq v} \frac{\tilde{U}_{vi} V_{iv}}{\epsilon_v - \epsilon_i} + \sum_{ai}^{i \neq v} \frac{V_{vi} [g_{iava}(0) - g_{iaav}(\delta E_{va})]}{\epsilon_v - \epsilon_i} + \sum_{ai}^{i \neq v} \frac{[g_{vaia}(0) - g_{vaai}(\delta E_{va})] V_{iv}}{\epsilon_v - \epsilon_i} \\
 & + \sum_{ai}^{i \neq a} \frac{V_{ai} [g_{ivav}(0) - g_{ivva}(-\delta E_{va})]}{\epsilon_a - \epsilon_i} + \sum_{ai}^{i \neq a} \frac{[g_{aviv}(0) - g_{avvi}(-\delta E_{va})] V_{ia}}{\epsilon_a - \epsilon_i} - \sum_{wa} V_{vw} g'_{wava}(\delta E_{va}) \\
 & - \sum_{ab} V_{ab} g'_{bvva}(-\delta E_{va}), \tag{9}
 \end{aligned}$$

with $\delta E_{va} = \epsilon_v - \epsilon_a$,

$$\begin{aligned}
 g_{ijkl}(E) \equiv & \alpha \int d^3x d^3y \frac{e^{i\sqrt{E^2+i\delta}|\vec{x}-\vec{y}|}}{|\vec{x}-\vec{y}|} \bar{\psi}_i(\vec{x}) \gamma_\mu \psi_k(\vec{x}) \\
 & \times \bar{\psi}_j(\vec{y}) \gamma^\mu \psi_l(\vec{y}), \tag{10}
 \end{aligned}$$

and $g'(E) = dg/dE$. Here v and a refer to the valence and core states, respectively, and the sum over i ranges over both positive- and negative-energy states. The excluded cases $i \neq v$ and $i \neq a$ are associated with the last two ‘‘derivative’’ terms. The indicated summations over w and b in these terms range only over the magnetic quantum number, with the states otherwise being identical with v and a , respectively. The numerical evaluation of ν^{1E} is straightforward, and results are presented in the sixth row of Table I. The sums of theoretical results up to this point are tabulated in the seventh row of Table I, while their differences with experiment are shown in the eighth row as ΔExpt , which are dominated by higher-order correlation corrections and should closely approximate the ν^{2E+} term.

The one-photon exchange matrix element ν^{1E} is defined in Feynman gauge in Eq. (9). Because we are using a local potential, results are gauge independent and are equivalent to the Coulomb gauge ones. Were that gauge to be used, transverse photon exchange neglected, and only positive-energy

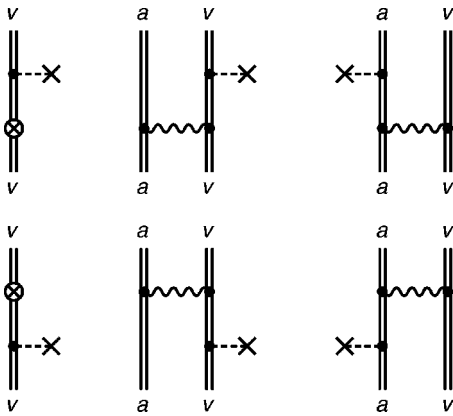


FIG. 1. Feynman diagrams for the one-photon exchange corrections to hyperfine splitting. The dashed line terminated with a cross indicates a hyperfine interaction and the symbol \otimes represents the counter potential. Exchange diagrams between the core and valence electrons are not shown here.

states summed over, the results of first-order MBPT would be recovered: this exercise is carried out and results are shown in the ninth row of Table I. The difference between ν^{1E} and first-order MBPT is tabulated in the last row of Table I as the Breit-QED term. This difference involves a number of effects, some of which could be incorporated into an MBPT treatment by inclusion of the instantaneous Breit interaction, and others which are field theoretic in origin, involving both the effect of negative-energy states and retardation in the transverse photon exchange term. We do not separate the various effects. While quite small for the light alkali metals, this difference becomes important for the heavier alkali metals. The fact that the Breit interaction gives significant contributions to hfs for the heavier alkali metals has also been noted in Refs. [19] and [20]. We now turn to the calculation of radiative corrections.

IV. RADIATIVE CORRECTIONS

The diagrams representing vacuum polarization (VP) contributions to hfs are shown in Fig. 2. We break this term up as

$$\nu^{\text{VP}} = \nu^{\text{VP}}(\text{V}) + \nu^{\text{VP}}(\text{PO}). \tag{11}$$

The first term, corresponding to Fig. 2(b), is referred to as a vertex (V) correction. It is given by

$$\begin{aligned}
 \nu^{\text{VP}}(\text{V}) = & \frac{e\alpha}{3\pi} \int_0^1 dx \frac{x(1-2x)(3-2x)}{1-x} \int d^3r \psi_v^\dagger(\vec{r}) \vec{\alpha} \cdot \vec{A}(\vec{r}) \\
 & \times \psi_v(\vec{r}) e^{-\frac{(mr)}{\sqrt{x(1-x)}}} \left[1 + \frac{mr}{\sqrt{x(1-x)}} \right] \tag{12}
 \end{aligned}$$

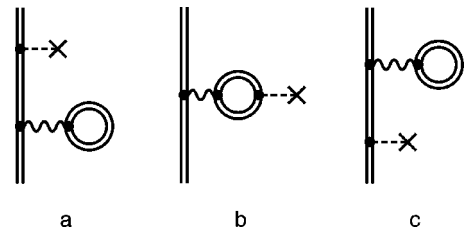


FIG. 2. Feynman diagrams for the vacuum polarization corrections to hyperfine splitting. The dashed line terminated with a cross indicates a hyperfine interaction.

TABLE II. Vacuum polarization (VP) and self-energy (SE) contributions to hfs in the alkali metals. QED is the sum of VP and SE: Units $(\alpha/\pi)E_F$.

	⁷ Li	²³ Na	³⁹ K	⁸⁷ Rb	¹³³ Cs	²¹² Fr
$\nu^{\text{VP}}(\text{V})$	0.025	0.088	0.152	0.301	0.479	0.896
$\nu^{\text{VP}}(\text{PO})$	0.026	0.103	0.193	0.464	0.904	2.753
VP sum	0.051	0.191	0.345	0.765	1.383	3.649
$\nu^{\text{SE}}(\text{PO})$	-0.044	-0.250	-0.490	-1.085	-1.789	-3.741
$\nu^{\text{SE}}(\text{A})$	-3.242	-1.293	-0.764	-0.436	-0.428	-0.639
$\nu^{\text{SE}}(\text{B})$	-276.505	-234.853	-240.151	-231.345	-229.325	-218.932
$\nu^{\text{SE}}(\text{C})$	8.916	9.011	9.232	9.289	9.380	9.360
$\nu^{\text{SE}}(\text{D})$	-0.004	-0.041	-0.076	-0.157	-0.240	-0.391
$\nu^{\text{SE}}(\text{E})$	271.178	227.228	231.548	221.828	219.201	208.095
SE sum	0.299	-0.198	-0.701	-1.906	-3.201	-6.248
QED	0.350	-0.007	-0.356	-1.141	-1.818	-2.599
ν^{BW}	-0.047	-0.212	-0.441	-1.327	-3.068	-11.643

and is tabulated in the first row of Table II. Figures 2(a) and 2(c) lead to the ‘‘perturbed orbital’’ (PO) terms, where the perturbed orbital is defined as

$$\psi_{\bar{v}}(\vec{r}) \equiv \sum_{i \neq v} \psi_i(\vec{r}) \frac{V_{iv}}{\epsilon_v - \epsilon_i}. \quad (13)$$

If the Uehling potential is defined as

$$U_{\text{VP}}(r) \equiv \frac{\alpha^2}{4\pi^2} \int_0^1 dy \frac{y^2(1-y^2/3)}{1-y^2} \times \int d^3x \frac{e^{-[2m|\vec{x}-\vec{r}|/\sqrt{(1-g^2)}]}}{|\vec{x}-\vec{r}|} \vec{\nabla}_x^2 \left[\frac{Z_{\text{eff}}(x)}{x} \right], \quad (14)$$

the PO contributions to vacuum polarization are

$$\nu^{\text{VP}}(\text{PO}) = \int d^3r [\psi_v^\dagger(\vec{r}) U_{\text{VP}}(r) \psi_{\bar{v}}(\vec{r}) + \psi_{\bar{v}}^\dagger(\vec{r}) U_{\text{VP}}(r) \psi_v(\vec{r})], \quad (15)$$

and are tabulated in the second row of Table II. Higher-order corrections to vacuum polarization, known as the Wichmann-Kroll terms [1], are very small in neutral atoms and will not be considered here. We note that for both $\nu^{\text{VP}}(\text{V})$ and $\nu^{\text{VP}}(\text{PO})$, the first term in the $Z\alpha$ expansion is $3/8\alpha(Z\alpha)E_F$ [7], which for $Z=3$ is $0.0258\alpha/\pi E_F$, in close agreement with our results for lithium. The sum of the two vacuum polarization contributions are tabulated in the third row of Table II.

Turning now to the more complicated self-energy calculation, we break it up into six parts,

$$\nu^{\text{SE}} = \nu^{\text{SE}}(\text{PO}) + \nu^{\text{SE}}(\text{A}) + \nu^{\text{SE}}(\text{B}) + \nu^{\text{SE}}(\text{C}) + \nu^{\text{SE}}(\text{D}) + \nu^{\text{SE}}(\text{E}). \quad (16)$$

The simplest part of this is the PO term, which comes from Figs. 3(a) and 3(c), and can be written as

$$\nu^{\text{SE}}(\text{PO}) = \int d^3x \int d^3y [\bar{\psi}_v(\vec{x}) \Sigma(\vec{x}, \vec{y}; \epsilon_v) \psi_{\bar{v}}(\vec{y}) + \bar{\psi}_{\bar{v}}(\vec{x}) \Sigma(\vec{x}, \vec{y}; \epsilon_v) \psi_v(\vec{y})], \quad (17)$$

where

$$\Sigma(\vec{x}, \vec{y}; E) = -ie^2 \int \frac{d^n k}{(2\pi)^n} \frac{e^{ik \cdot (\vec{x} - \vec{y})}}{k^2 + i\delta} \gamma_\mu S_F(\vec{x}, \vec{y}; E - k_0) \gamma^\mu. \quad (18)$$

The self-energy function Σ is defined in $n=4-\epsilon$ dimensions to regulate ultraviolet divergences and a self-mass counter-term is assumed. The calculation then reduces to the kind of self-energy calculation described in Ref. [14], and results are tabulated in the fourth row of Table II.

The vertex diagram of Fig. 3(b) is given by

$$E_v = -4\pi i \alpha \int d^3x d^3y d^3z \int \frac{d^n k}{(2\pi)^n} \frac{e^{ik \cdot (\vec{x} - \vec{z})}}{k^2 + i\delta} \bar{\psi}_v(\vec{x}) \gamma_\mu \times S_F(\vec{x}, \vec{y}; \epsilon_v - k_0) V(\vec{y}) S_F(\vec{y}, \vec{z}; \epsilon_v - k_0) \gamma^\mu \psi_v(\vec{z}). \quad (19)$$

If a spectral decomposition of the two-electron propagators is made and the d^3k integration carried out analytically, an alternative form for the vertex term results

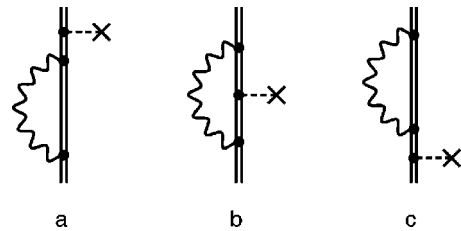


FIG. 3. Feynman diagrams for the self-energy corrections to hyperfine splitting. The dashed line terminated with a cross indicates a hyperfine interaction.

$$E_v = i \sum_{mn} \int \frac{dk_0}{2\pi} \times \frac{V_{mn} g_{vnmv}(k_0)}{[\epsilon_v - k_0 - \epsilon_m(1-i\delta)][\epsilon_v - k_0 - \epsilon_n(1-i\delta)]}. \quad (20)$$

The vertex term can be rendered finite by subtracting the same form with the bound-state propagators replaced by free propagators, $E_v = [E_v - E_v(\text{free})] + E_v(\text{free}) = \Delta E_v + \nu^{\text{SE}}(A)$. This gives rise to the $\nu^{\text{SE}}(A) = E_v(\text{free})$ term which is evaluated in momentum space,

$$\nu^{\text{SE}}(A) = -4\pi i \alpha \int d^3 p_2 d^3 p_1 \int \frac{d^n k}{(2\pi)^n} \frac{1}{k^2 + i\delta} \bar{\psi}_v(\vec{p}_2) \gamma_\mu \frac{1}{\not{p}_2 - \not{k} - m} V(\vec{p}_2 - \vec{p}_1) \frac{1}{\not{p}_1 - \not{k} - m} \gamma^\mu \psi_v(\vec{p}_1), \quad (21)$$

where the Fourier transform of $V(\vec{r})$ is given by

$$V(\vec{q}) = i e \vec{\gamma} \cdot \frac{\vec{\mu} \times \vec{q}}{8\pi^3 |\vec{q}|^2}. \quad (22)$$

Standard manipulations allow the $d^n k$ integration to be performed, with the result

$$\begin{aligned} \nu^{\text{SE}}(A) &= \frac{\alpha}{2\pi} \left[\frac{C}{\epsilon} - 1 \right] E_F - \frac{\alpha}{2\pi} \int_0^1 \rho d\rho \int_0^1 dx \int d^3 p_2 d^3 p_1 \bar{\psi}_v(\vec{p}_2) V(\vec{p}_2 - \vec{p}_1) \psi_v(\vec{p}_1) \ln(\Delta_v / m^2) \\ &\quad + \frac{\alpha}{4\pi} \int_0^1 \rho d\rho \int_0^1 dx \int d^3 p_2 d^3 p_1 \bar{\psi}_v(\vec{p}_2) N_v \psi_v(\vec{p}_1) (1/\Delta_v), \end{aligned} \quad (23)$$

where $C = (4\pi)^{\epsilon/2} \Gamma(1 + \epsilon)$,

$$\begin{aligned} \Delta_v &= \rho^2 E^2 + \rho(m^2 - E^2) + \rho x \vec{p}_1^2 + \rho(1-x) \vec{p}_2^2 \\ &\quad - \rho^2 |x \vec{p}_1 + (1-x) \vec{p}_2|^2, \end{aligned} \quad (24)$$

and

$$\begin{aligned} N_v &= \gamma_\mu \{ \not{p}_2 [1 - \rho(1-x)] - \not{p}_1 \rho x + m \} V(\vec{q}) \{ \not{p}_1 (1 - \rho x) \\ &\quad - \not{p}_2 \rho(1-x) + m \} \gamma^\mu. \end{aligned} \quad (25)$$

The first term in Eq. (23) is ultraviolet divergent and will be shown to cancel in the following. The remaining finite parts of $\nu^{\text{SE}}(A)$ are readily evaluated numerically, and results for this term are tabulated in the fifth row of Table II.

The ‘‘subtracted’’ term ΔE_v is evaluated in coordinate space, with the k_0 integration done numerically after the Wick rotation $k_0 \rightarrow i\omega$. Evaluation of this term will be discussed later. Here, we note that the Wick rotation surrounds poles when bound-state propagators are present and leads to the extra expression

$$\begin{aligned} \nu^{\text{SE}}(B) &= - \sum_{m \neq n}^{m \neq n} A_m \frac{g_{vnmv}(\epsilon_v - \epsilon_m) V_{mn}}{\epsilon_n - \epsilon_m} \\ &\quad - \sum_{m \neq n}^{m \neq n} A_n \frac{g_{vnmv}(\epsilon_v - \epsilon_n) V_{mn}}{\epsilon_m - \epsilon_n}, \end{aligned} \quad (26)$$

where A_i is 1 if the state i has been encircled, 1/2 if a semi-circle is used to circumvent it, and 0 otherwise. We have suppressed a double-pole term associated with the case of $m = n$ in Eq. (20) that will be combined with those from the ‘‘side’’ diagrams, Figs. 3(a) and 3(c), discussed below. The calculation of $\nu^{\text{SE}}(B)$ is carried out with finite basis set techniques [21], with the main numerical concern being making the basis set large enough so that all bound states are represented accurately. Results are tabulated in the sixth row of Table II.

Turning back to the side diagrams of Figs. 3(a) and 3(c), we note that they give rise to the already treated PO terms, but in addition contribute the term

$$\begin{aligned} E_s &= 4\pi i \alpha E_F \int d^3 x d^3 y d^3 z \int \frac{d^n k}{(2\pi)^n} \frac{e^{i\vec{k} \cdot (\vec{x} - \vec{z})}}{k^2 + i\delta} \bar{\psi}_v(\vec{x}) \\ &\quad \times \gamma_\mu S_F(\vec{x}, \vec{y}; \epsilon_v - k_0) \gamma_0 S_F(\vec{y}, \vec{z}; \epsilon_v - k_0) \gamma^\mu \psi_v(\vec{z}), \end{aligned} \quad (27)$$

which accounts for the change in the self-energy from the shift in the energy due to hfs. As with the vertex term, we first subtract a term with the bound-state electron propagators replaced with free-electron propagators such that $E_s = \Delta E_s + \nu^{\text{SE}}(C)$. This gives, in momentum space, the contribution

$$\begin{aligned}
\nu^{\text{SE}}(C) = & -\frac{\alpha}{2\pi} \left[\frac{C}{\epsilon} - 1 \right] E_F \\
& + \frac{\alpha}{2\pi} E_F \int_0^1 \rho d\rho \int d^3p \bar{\psi}_v(\vec{p}) \gamma_0 \psi_v(\vec{p}) \ln(\Delta_s/m^2) \\
& + \frac{\alpha}{4\pi} E_F \int_0^1 \rho d\rho \int d^3p \bar{\psi}_v(\vec{p}_2) N_s \psi_v(\vec{p}) (1/\Delta_s),
\end{aligned} \tag{28}$$

where

$$\Delta_s = \rho^2 (\epsilon_v^2 - \vec{p}^2) + \rho(m^2 - \epsilon_v^2 + \vec{p}^2) \tag{29}$$

and

$$N_s = \gamma_\mu [\not{p}(1-\rho) + m] \gamma_0 [\not{p}(1-\rho) + m] \gamma^\mu. \tag{30}$$

The divergent term in Eq. (28) cancels with the divergent term in Eq. (23) and the finite parts of $\nu^{\text{SE}}(C)$ are tabulated in the seventh row of Table II.

We perform a Wick rotation on the ‘‘subtracted’’ term ΔE_s which leads to a derivative term when double poles are encircled. There are also double-pole terms from the neglected vertex term mentioned above, and we combine them into

$$\nu^{\text{SE}}(D) = \sum_m A_m g'_{vmmv} (\epsilon_v - \epsilon_m) (V_{mm} - V_{vv}) \tag{31}$$

tabulated in the eighth row of Table II.

A complication in bound-state calculations of radiative corrections is the presence of singularities associated with the propagator, when represented as a sum over states, being degenerate in energy with the valence state. As in our previous work [12], we regulate this singularity by changing the valence energy by a factor $1 - \delta$. It is present in the Wick-rotated vertex and side ‘‘subtracted’’ terms ΔE_v and ΔE_s , but cancels in the sum. For this reason we evaluate these terms together in coordinate space with partial wave expansions. The combined results are tabulated in the ninth row of Table II as the $\nu^{\text{SE}}(E)$ term. The summed self-energy results shown in the tenth row of Table II, together with the vacuum polarization results shown in the third row, constitute the radiative corrections to the ground-state hfs of the alkali metals and are the principal results of this paper.

V. DISCUSSION

We first compare our radiative correction results shown in the eleventh row of Table II to those obtained for hydrogenic ions [4]. Those results, which were extended down to $Z=1$ in Ref. [8], showed that the QED correction starts off close to $\alpha/2\pi E_F$, reduces in magnitude until it changes sign around $Z=10$, and then goes more and more negative. This behavior persists in the neutral alkali metals considered here, which is not surprising considering that hfs is a short-distance effect that should be sensitive to the overall nuclear charge despite the fact that the electronic wave function in

general sees a highly screened nuclear charge. It is also clear from this work that while it is a good approximation to use the Schwinger correction for lithium, by the time sodium is considered, the effect already almost cancels between vacuum polarization and self-energy, and in the case of cesium, the effect is opposite in sign to, and four times larger than the Schwinger correction.

Whereas E_F for a one-electron atom or ion accounts for all nonradiative corrections, in the many-electron case, both the Hartree-Fock potential [22] and the Kohn-Sham potential used here tend to understate the hfs significantly in lowest-order calculations. This complicates the discussion of radiative corrections, which are much smaller than the difference between theory and experiment. Indeed, as shown in Table I, even with the first-order correction ν^{1E} included, theory is still quite different from experiment, as can be seen from the term ΔExpt , which should be roughly equal to the size of the higher-order correlation corrections term ν^{2E+} neglected here. We have chosen to present our results in terms of $\alpha/\pi E_F$. While E_F is smaller than experiment for the Kohn-Sham potential, we consider it likely that the approximation of replacing E_F with the full hfs (i.e., $E_F = \nu^{(0)} + \nu^{1E} + \nu^{2E+}$) is a good one, though proof of this would involve complex higher-order calculations that include correlation and QED together.

It would clearly be of interest to compare with experiment and determine whether the radiative corrections calculated here are indeed present. In fact, in the one case, lithium, where accurate wave functions are available, the calculated 2s hfs [23] differs from experiment by only 93 ppm, a factor of 10 smaller than the Schwinger term, which clearly indicates its presence. However, it should be cautioned that the same calculation also gives a 3s hfs, which disagrees with experiment by a factor of 14 times the Schwinger correction. As for the other alkali metals, calculations of many-body corrections to E_F are much less precise, making it impossible to detect radiative corrections to hfs in these atoms at the present moment. Indeed, a many-body treatment of E_F using coupled-cluster theory with single-double excitations was shown in Ref. [20] to be quite inaccurate, and while the inclusion of a set of triple excitations in the same work improved the agreement between theory and experiment to the 1 percent level, further extensions of the method are clearly needed. It is notable that the highest claimed accuracy for parity nonconserving transitions in cesium [24], a calculation into which extensive efforts have been made, is 0.5 percent, which is still too large for our purpose. Therefore, the radiative corrections calculated here for the heavier alkali metals, while relatively large, cannot, with present many-body methods, be said to be definitely present.

Even when many-body methods improve in accuracy, it may still be difficult to detect the radiative corrections calculated here because of the question of the distribution of nuclear magnetism. In the last row of Table II, the contributions ν^{BW} , first shown in Table I in units of MHz, are presented in units of $\alpha/\pi E_F$. It can be seen that they are comparable to the QED corrections calculated here. As our derivation of ν^{BW} was fairly unsophisticated, it is thus possible that the same situation encountered in highly-charged

bismuth ions discussed in the introduction, where uncertainties in the distribution of nuclear magnetism mask QED effects, will be encountered for the neutral alkali metals. However, as pointed out in Refs. [11] and [12], having more than one hyperfine interval to compare with theory allows this uncertainty to be greatly minimized or even completely avoided. While the additional hfs in the case of $^{209}\text{Bi}^{82+}$ was not measured with sufficiently high accuracy to be sensitive to radiative corrections, for the neutral alkali metals there are usually several accurately measured excited state hyperfine intervals. As the many-body techniques used for the accurate calculation of the ground-state hfs are just as applicable to excited-state hfs, the most promising method to unambiguously detect the large radiative corrections calculated here is

the application of the next generation of many-body techniques to two or more states of the same atom. Further experimental work on accurate determinations of hyperfine intervals of excited states of the alkali metals would be of considerable value for such an approach.

ACKNOWLEDGMENTS

The work of J.S. was supported in part by NSF Grant No. PHY-0097641. The work of K.T.C. was performed under the auspices of the U.S. Department of Energy at the University of California, Lawrence Livermore National Laboratory under Contract No. W-7405-ENG-48.

-
- [1] E. Wichmann and N. Kroll, *Phys. Rev.* **101**, 343 (1956).
 [2] G.E. Brown and D.F. Mayers, *Proc. R. Soc. London, Ser. A* **251**, 105 (1959).
 [3] U.D. Jentschura, P.J. Mohr, and G. Soff, *Phys. Rev. Lett.* **82**, 53 (1999).
 [4] H. Persson, S.M. Schneider, W. Greiner, G. Soff, and I. Lindgren, *Phys. Rev. Lett.* **76**, 1433 (1996); S.A. Blundell, K.T. Cheng, and J. Sapirstein, *Phys. Rev. A* **55**, 1857 (1997); V.M. Shabaev, M. Tomaselli, T. Kühn, A.N. Artemyev, and V.A. Yerokhin, *ibid.* **56**, 252 (1997).
 [5] I. Klaft, S. Borneis, T. Engel, B. Fricke, R. Grieser, G. Huber, T. Kühn, D. Marx, R. Neumann, S. Schröder, P. Seelig, and L. Völker, *Phys. Rev. Lett.* **73**, 2425 (1994).
 [6] J. Schwinger, *Phys. Rev.* **75**, 898 (1949).
 [7] N. Kroll and F. Pollack, *Phys. Rev.* **84**, 594 (1951); R. Karplus, A. Klein, and J. Schwinger, *ibid.* **84**, 597 (1951).
 [8] S.A. Blundell, K.T. Cheng, and J. Sapirstein, *Phys. Rev. Lett.* **78**, 4914 (1997).
 [9] A. Bohr and V.F. Weisskopf, *Phys. Rev.* **77**, 94 (1950).
 [10] M. Tomaselli, T. Kühn, P. Seelig, G. Holbrow, and E. Kankeleit, *Phys. Rev. C* **58**, 1524 (1998).
 [11] V.M. Shabaev, M.B. Shabaeva, I.I. Tupitsyn, and V.A. Yerokhin, *Hyperfine Interact.* **114**, 129 (1998).
 [12] J. Sapirstein and K.T. Cheng, *Phys. Rev. A* **63**, 032506 (2001).
 [13] P. Beiersdorfer, A.L. Osterheld, J.H. Scofield, J.R. Crespo López-Urritia, and K. Widmann, *Phys. Rev. Lett.* **80**, 3022 (1998).
 [14] J. Sapirstein and K.T. Cheng, *Phys. Rev. A* **66**, 042501 (2002).
 [15] In *Table of Isotopes*, 8th ed., edited by R.B. Firestone and V. S. Shirley (Wiley, New York, 1998).
 [16] W.R. Johnson and G. Soff, *At. Data Nucl. Data Tables* **33**, 405 (1985).
 [17] G.H. Fuller and V.W. Cohen, *Nucl. Data, Sect. A* **5**, 433 (1969).
 [18] A. Coc *et al.*, *Phys. Lett.* **163B**, 66 (1985).
 [19] A. Derevianko, *Phys. Rev. A* **65**, 012106 (2000).
 [20] M.S. Safronova, W.R. Johnson, and A. Derevianko, *Phys. Rev. A* **60**, 4476 (1999).
 [21] W.R. Johnson, S.A. Blundell, and J. Sapirstein, *Phys. Rev. A* **37**, 307 (1988).
 [22] W.R. Johnson, M. Idrees, and J. Sapirstein, *Phys. Rev. A* **35**, 3218 (1987).
 [23] Zong-Chao Yan, D.K. McKenzie, and G.W.F. Drake, *Phys. Rev. A* **54**, 1322 (1996).
 [24] V.A. Dzuba, V.V. Flambaum, and J.S.M. Ginges, e-print hep-th/0204134.